CHIN. PHYS. LETT. Vol. 37, No. 6 (2020) 068501

Mid-Infrared InAs/GaSb Superlattice Planar Photodiodes Fabricated by Metal–Organic Chemical Vapor Deposition *

Yu Zhao(赵宇)[1], Yan Teng(滕奘)[1], Jing-Jun Miao(缪静君)[1], Qi-Hua Wu(吴启花)[1], Jing-Jing Gao(高晶晶)[1], Xin Li(李欣)[1], Xiu-Jun Hao(郝修军)[1], Ying-Chun Zhao(赵迎春)[2], Xu Dong(董旭)[2], Min Xiong(熊敏)[2], Yong Huang(黄勇)[1]**

[1]*Key Lab of Nanodevices and Applications, Suzhou Institute of Nano-tech and Nano-bionics, Chinese Academy of Sciences, Suzhou 215123, China*

[2]*Nano-fabrication Facility, Suzhou Institute of Nano-tech and Nano-bionics, Chinese Academy of Sciences, Suzhou 215123, China*

(Received 5 March 2020)

Mid-wavelength infrared planar photodiodes were demonstrated, in which both the epitaxy growth of InAs/GaSb superlattices and the thermal diffusion of p-type dopant were performed in production-scale metal–organic chemical vapor deposition reactors. The formation of a planar homojunction was confirmed by secondary ion mass spectroscopy and its I–V characteristics. A cut-off wavelength around 5 μm was determined in 77 K optical characterization, and photo-current as high as 600 nA was collected from a reverse-biased planar diode of 640 μm diameter. These preliminary results were obtained despite the structural degradation revealed by x-ray diffraction, and we attribute the degradation to the concert of thermal annealing and high Zn concentration behind the diffusion front.

PACS: 85.60.Gz, 73.40.Kp, 81.15.Gh DOI: 10.1088/0256-307X/37/6/068501

InAs/GaSb type-Ⅱ superlattice (SL) as an infrared detecting material is highly appreciated for its wide wavelength coverage, great flexibility in band gap engineering and continuously improving device performance approaching that of commercialized HgCdTe components.[1] In addition, SL-based devices are also endowed by Ⅲ–V based technologies with its large format, superior uniformity, high repeatability and excellent production yield.[2–4]

Nevertheless, surface leakage is a prominent bottleneck limiting the performance of InAs/GaSb based SL detectors. It is an important source of inhomogeneity in detector arrays and causes hot pixels. For mesa-type devices employed in current SL detectors, surface leakage is often correlated with damage and contamination introduced during sidewall etching or any subsequent technological processes. It cannot be completely eradicated despite the various efforts made in sidewall passivation.[5–7] Planarization of the p–n junction is a possible solution to sidewall related problems: by selectively introducing dopants into a bulk material by either ion implanting or thermal diffusion, lateral p–n junctions are formed so that the sheer existence of sidewall is eliminated. Planar technologies have been successfully applied to commercialized detectors like InP/InGaAs short-wavelength infrared avalanche diodes,[8] HgCdTe[9] and InSb[10] mid-wavelength infrared (MWIR) detector arrays. However, there have been very few investigations on InAs/GaSb SL-based planar devices,[11,12] posing concerns such as the effectiveness of the *ex situ* dopants and the intactness of the SL quality during implantation or diffusion.

We recently demonstrated the feasibility of growing high-quality mid-wavelength InAs/GaSb superlattice (MWSL) and long-wavelength superlattice (LWSL) detectors using a production-capable metal–organic chemical vapor deposition (MOCVD) system.[13–15] On the other hand, MOCVD is a proven technology in planar junction fabrication by selective zinc (Zn) diffusion into Ⅲ–V materials under a controlled process temperature and chemical ambient.[16] In this Letter, we report our initial efforts in advancing the manufacturability of InAs/GaSb SL based detectors by implementing planar photodiodes, of which both the epitaxial growth and selectively doped planar junction were achieved in MOCVD reactors. First, the diffusion of Zn in bulk InAs, GaSb and InAs/GaSb SLs will be compared. Then, the characteristics of planar SL diodes are examined alongside photoconductors where no junctions are formed.

The InAs/GaSb MWSLs wafers studied were grown in an Aixtron 2400G3 MOCVD reactor and detailed growth conditions can be found elsewhere.[13] On an InAs substrate of undoped n-type, 1000-nm-thick undoped mid-wavelength superlattices (MWSLs) were deposited at 530 ℃. The SLs were terminated by a GaSb sublayer of 5 nm thickness to mitigate surface electron accumulation commonly found in InAs-rich materials.[6] In order to achieve a cut-off wavelength around 5 μm, the MWSLs consist of InAs and GaSb sublayers of 11 and 9 monolayers

*Supported by the National Natural Science Foundation of China (Grant Nos. 61874179, 61804161, and 61605236).
**Corresponding author. Email: yhuang2014@sinano.ac.cn
© 2020 Chinese Physical Society and IOP Publishing Ltd

(MLs) in thickness, respectively. A background n-type concentration of $5 \times 10^{15}\,\mathrm{cm}^{-3}$ and a sheet resistance of $650\,\Omega/\square$ were determined for the MWSLs by 77 K Hall measurement made on lift-off[17] epitaxy layers.

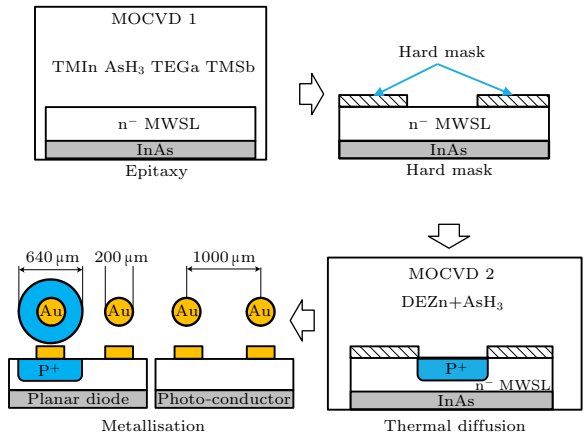

Fig. 1. Fabrication process flow of InAs/GaSb SL-based planar diodes.

The diffusion process was run in a Thomas-Swan MOCVD reactor equipped with a closed coupled shower head and a 6 × 2-inch rotational graphite susceptor. Thermal diffusion of Zn was carried out under 500 ℃ for 30 min in a H_2-based ambient consisting of DEZn as dopant and group-V precursor AsH_3 or TMSb to prevent incongruent desorption.[18] All process parameters followed recipes such that zoned susceptor temperatures, reactor pressure and gas flows were actively controlled throughout the process, even during cooling down. To improve run-to-run repeatability, the reactor was coated with the same recipe prior to an experimental run. An undoped InAs substrate, an MWSL wafer for unselective doping and the selectively doped MWSL wafer described below were processed under exactly the same recipe, while a GaSb substrate was diffused under a modified recipe where TMSb was used in place of AsH_3. Profiles of Zn in these materials were examined by a time-of-flight secondary ion mass spectroscopy (SIMS) system, where cations were analyzed by Cs^+ ions.

Selectively doped planar photodiodes were fabricated following the process illustrated in Fig. 1. Before any subsequent technological process, a set of markers were etched on the sample surface to enable the alignment of diffusion windows and electrodes. Crack-free SiN_x hard mask was deposited on MWSLs using plasma enhanced chemical vapor deposition, and diffusion windows were opened by standard photolithography and dry etching. Then the patterned sample was transferred into the MOCVD reactor for selective diffusion. Zn species entered the open areas and turned surface n^- MWSL layers into p^+ MWSLs. After the diffusion process, the hard mask was removed in HF-based etchant to set the surface free from Zn-containing residuals. For simplicity, no passivation layer was regrown. Electrodes were realized by the deposition of a Ti/Pt/Au stack and standard metal lift-off. Good electrical contact was verified by transmission line measurements made at room temperature. Planar devices presented in this study have diffusion windows of 640 μm diameter. The p-contacts of planar diodes refer to those sitting on diffused zones while the n-contacts are those formed on adjacent non-diffused regions. For proof of concept only, instead of being ring-shaped the electrodes are circular pads of 200 μm diameter equally spaced by 1000 μm. As a result, both the electrical and optical areas are undefined. Alongside the planar diodes, the same set of electrodes were deposited on an MWSL wafer that has not undergone Zn diffusion. By connecting electrodes on this 'blank' wafer, a comparative set of photoconductors were made. The sample wafers were then diced, wire-bound and mounted in a liquid nitrogen cooled Dewar for further characterizations.

Depth profiles of Zn in InAs, GaSb bulk material and the planar diode are presented in Fig. 2(a). The atomic concentration of Zn was determined by assuming constant ratios between the yield of $CsIn^+/CsZn^+$ ($CsGa^+/CsZn^+$) across these samples. Diffused at the same temperature, GaSb seemed to have achieved the highest surface Zn concentration approaching $1 \times 10^{21}\,\mathrm{cm}^{-3}$ while InAs had the lowest concentration of about $1 \times 10^{19}\,\mathrm{cm}^{-3}$ behind its diffusion front. For InAs and GaSb, the observed concentrations agree with the solubility of Zn found in the literature.[19,20] For the InAs/GaSb MWSL, it has attained an intermediate concentration of $5 \times 10^{19}\,\mathrm{cm}^{-3}$ that an intuitive interpolation of Zn's solubility could explain. Such 1×10^{19}–$1 \times 10^{20}\,\mathrm{cm}^{-3}$ atomic Zn concentrations achieved by thermal diffusion process are much higher than those achieved during *in situ* doping.

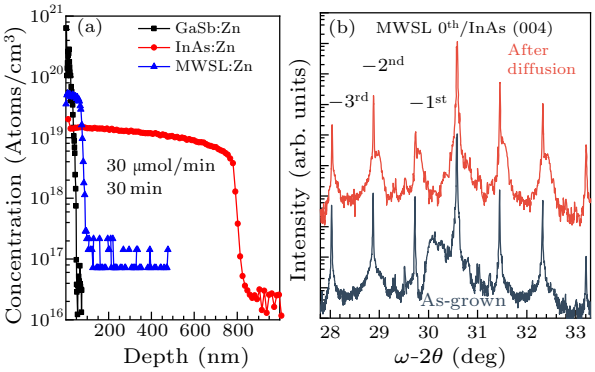

Fig. 2. SIMS profiles of Zn in the InAs substrate, GaSb substrate and selectively doped region in a planar diode (a). XRD patterns of MWSL, before and after unselective diffusion of Zn (b).

The sputtering depth was determined through the measurement of sputtering craters on InAs and GaSb substrates and by marker elements in the case of MWSL:Zn. For the same diffusion time, Zn diffusion front has invaded 800 nm into InAs but only 60 nm into the GaSb substrate. This is an apparent result of

the much higher diffusion coefficient of Zn in InAs[21] than in GaSb.[22] However, oxides on the GaSb substrate may also have intervened.[23] It is difficult to remove oxide by thermal annealing at 500 ℃ alone, and progress of diffusion is subject to the state of surface and thus any prior chemical treatment. For the case of MWSL:Zn, abundant Zn was detected up to a depth of 90 nm and the signal plunged into the level of detection background thereafter. Since Zn is a proven p-type dopant in both InAs and GaSb materials, a junction depth of about 90 nm is thus determined for the planar devices. Nevertheless, simple interpolation suggests that InAs/GaSb SLs would have varying Zn diffusion capabilities depending on their compositions: faster in InAs-rich LWSLs but slower in MWSLs. To ensure good reproducibility of Zn diffusion, future experiment should be carried out with SLs encapsulated by a thin InAs layer which allows desorption of surface oxides as early as 300 ℃ in the presence of H_2.[24]

Figure 2(b) shows the XRD patterns of an MWSL wafer, before and after unselective thermal diffusion. The as-grown pattern shows sharp satellite peaks from the MWSLs and the (004) reflection from the InAs substrate. While all these features are mostly retained in the 'diffused' pattern, the encapsulating GaSb sublayer disappeared and all satellites were broadened; while the distance between the satellites was kept constant, copies of the original ones were translated to higher diffraction angles. We interpret such results as slight reduction of the SLs' average lattice constant. It is inferred from the sharp satellites in the diffused sample that the majority of SLs are intact and only surface layers of high Zn concentration are affected by the diffusion process. In fact, the InAs-based MWSL with GaAs-type interfaces have already endured growth temperatures as high as 530 ℃ for a few hours, no trace of degradation can be discerned in the as-grown XRD pattern. Such resistance against high temperature annealing is also observed in co-deposited MWSL:Zn layers having a hole concentration up to $5 \times 10^{18}\,\mathrm{cm}^{-3}$ in an n-on-p structure. We believe that the lattice contraction in the diffused sample is a result of inter-diffusion of Ga–In or even the formation of Zn-compound, which was activated by the synergy of high temperature annealing and saturated Zn incorporation.[25,26] This would probably be mitigated by using moderate diffusion conditions, *i.e.*, either lower diffusion temperature or moderate DEZn dosage.

Dark I–V characteristics of the planar diodes and companion photoconductors were recorded at 77 K. Since both their electrodes are made to be circular, the effective area for carrier collection is undefined; quantities in Figs. 3(a) and 3(b) are presented in current and resistance rather than densities. Unsurprisingly, the photoconductor showed perfectly symmetric I–V curve, and a linear resistance value of 3.2 kΩ that is mostly held constant throughout the probed range of bias voltages. For the planar diode, its rectifying I–V curve confirmed the formation of planar junction. It has harvested 1.5 decade lower dark current (5×10^{-6} A at −0.2 V) than the photoconductor devices and thus linear or differential resistance enhanced to the same extent ($6.0 \times 10^4\,\Omega$ at 0 V). For the photoconductor, the measured linear resistance actually coincided with a calculated value of $R = \rho_s L/W$, in which ρ_s is the sheet resistance acquired by Hall measurement, L is the separation between two pads (∼1000 μm) and W the dimension of a metal pad (200 μm). Such a coincidence suggests that the current took the shortest path between the two pads and it gives a rough estimation for the dimensions of the effective active region.

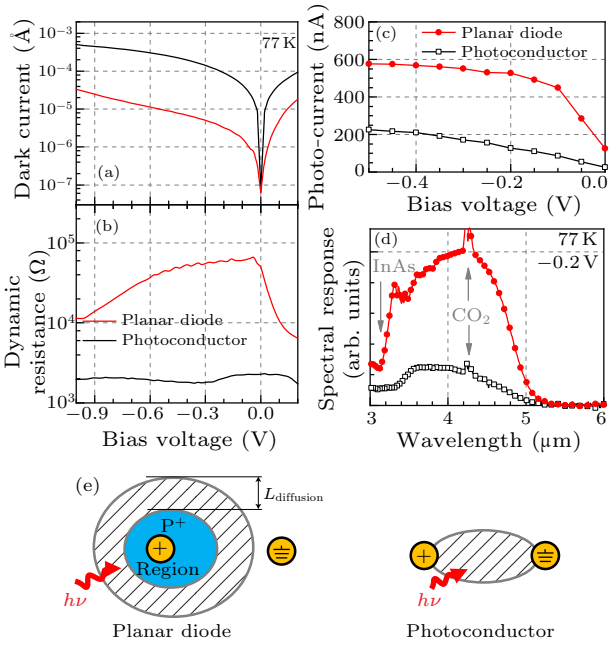

Fig. 3. Dark I–V characteristics (a) and differential resistance (b) of a planar diode and a photoconductor. Note that the devices are characterized by current/resistance rather than current density/resistance×area product. Photo-current (c) and relative response spectra (d) taken from a planar diode and a non-diffused photoconductor. Schematic explanations to different behaviors in photo-carrier collection are given in (e).

Response spectra were recorded by a Fourier transform spectrometer system where various corrections were applied to its raw data. As is shown in Fig. 3(d), both the devices have shown cut-off wavelengths close to 5 μm at −0.2 V bias. Under the illumination of a 600 K blackbody, absolute values of the photo-current collected by these devices were picked up as voltage output of a synchronous AM demodulation setup. The photoconductor again showed linear and symmetric characteristics, rendering 150 nA photocurrent under −0.2 V bias. For the planar diode, its photo-current increases at larger reverse bias and it tends to saturate at a level of about 580 nA for reverse bias voltages

greater than −0.4 V. The fact that the planar diode was able to harvest more photo-current than its photoconductor counterpart was probably a result of a much larger effective device area. As schematically illustrated in Fig. 3(e), the planar diode could capture photo-carriers generated beneath the p-region, in the depletion region and another peripheral region, of which the area is dictated by the diffusion length of holes in n^--MWSL. By assuming an overestimated 40% external quantum efficiency achieved by the planar diode, we estimated an effective optical area equivalent to a disc of 980 μm diameter. Since the depletion region does not expand dramatically, the larger collection area is attributed to a sufficiently large lateral diffusion length of photo-carriers in MWSLs. A lateral diffusion length of 170 μm is consistent with another ongoing investigation of ours, and its order of magnitude also agrees with the values reported for materials grown by molecular epitaxy techniques.[27] Although a large diffusion length of minority carrier is highly desired for many photodetectors, elevated lateral diffusion length may jeopardize the spatial resolution of a detector array and limit its pixel density. Additional measures for electrical isolation are to be taken in pursuit of planar InAs/GaSb SL detectors.

In summary, we have demonstrated an InAs/GaSb SLs based planar diode, of which both the epitaxy growth and the thermal diffusion p-type dopant were achieved in MOCVD reactors at temperatures over 500 ℃. A Zn concentration as high as 5×10^{19} cm^{-3} and a diffusion depth of 90 nm has been achieved by diffusion of Zn into InAs/GaSb SLs. Deviation from the original SLs was identified for the diffused material and it was attributed to In–Ga inter-diffusion activated by both the high Zn concentration and the elevated process temperature. Despite that, a planar device fabricated by selective Zn-doping has attained normal rectifying behavior, lower dark current and higher resistance as compared to its non-diffused photoconductor counterpart. Having a p-window of 640 μm diameter, the planar diode shows a dark current of 5×10^{-6} A and a differential resistance of $6 \times 10^4\,\Omega$ under −0.2 V bias. In photo-response, the planar diode has shown a cut-off wavelength over 5 μm, and it has attained I–V characteristics typical to a biased photodiode. Although the performance of this original planar diode is not yet comparable with mature mesa devices, improvements are expected once proper passivation and reinforced electrical isolation are implemented in future exploitation of InAs/GaSb SL-based planar devices.

The authors are grateful to Rong Huang for the SIMS analyses performed from the Vacuum Interconnected Nanotech Workstation (Nano-X), Suzhou Institute of Nanotech and Nano-bionics.

References

[1] Rogalski A, Martyniuk P and Kopytko M 2017 *Appl. Phys. Rev.* **4** 031304
[2] Forrai D et al 2018 *Infrared Phys. & Technol.* **95** 164
[3] Fastenau J M et al 2013 *Infrared Phys. & Technol.* **59** 158
[4] Liu A W K et al 2015 *Proc. SPIE* **9451** 94510T
[5] Gin A et al 2004 *Thin Solid Films* **447** 489
[6] Lowe M J et al 2002 *J. Cryst. Growth* **237** 196
[7] Chen G et al 2013 *Appl. Phys. Lett.* **103** 223501
[8] Dixon P et al 2009 *Proc. SPIE* **7307** 730706
[9] Wollrab R et al 2011 *J. Electron. Mater.* **40** 1618
[10] Shtrichman I et al 2007 *Proc. SPIE* **6542** 65423M
[11] Rajavel R et al 2009 *Proc. SPIE* **7298** 72981S
[12] Bogdanov S 2014 *PhD Dissertation* (Evanston: Northwestern University)
[13] Huang Y et al 2017 *IEEE J. Quantum Electron.* **53** 2740121
[14] Teng Y et al 2019 *IEEE Photon. Technol. Lett.* **31** 185
[15] Zhao Y et al 2020 *IEEE Photon. Technol. Lett.* **32** 19
[16] Pitts O J et al 2012 *International Conference on Indium Phosphide and Related Materials* (Santa Barbara, CA, USA 27–30 August 2012) p 225
[17] Cervera C et al 2009 *J. Appl. Phys.* **106** 033709
[18] Wang T et al 2019 *Appl. Phys. Express* **12** 122009
[19] da Cunha S F and Bougnot J 1974 *Phys. Status Solidi A* **22** 205
[20] Iwamura Y and Watanabe N 2000 *Jpn. J. Appl. Phys.* **39** 5740
[21] Khald H, Mani H and Joullie A 1988 *J. Appl. Phys.* **64** 4768
[22] Nicols S P et al 2001 *Physica B* **308** 854
[23] Schlegl T, Sulima O V and Bett A W 2004 *AIP Conf. Proc.* **738** 396
[24] Lyadov Y et al 2010 *J. Appl. Phys.* **107** 053518
[25] van Gurp G J et al 1990 *J. Appl. Phys.* **67** 2919
[26] Ky N H et al F K 1993 *J. Appl. Phys.* **73** 3769
[27] Plis E et al 2008 *Appl. Phys. Lett.* **93** 123507